Field and laboratory estimates of pore size properties and hydraulic characteristics for subarctic organic soils

Sean K. Carey,[1]* William L. Quinton[2] and Neil T. Goeller[3]

[1] *Department of Geography and Environmental Studies, Carleton University, Ottawa, Ontario, Canada K1S 5A5, Canada*
[2] *Cold Regions Research Centre, Wilfrid Laurier University, Waterloo, Ontario, Canada N2L 3C5, Canada*
[3] *Department of Geography, Simon Fraser University, Burnaby, British Columbia, Canada V5A 1C6, Canada*

Abstract:

Characterizing active and water-conducting porosity in organic soils in both saturated and unsaturated zones is required for models of water and solute transport. There is a limitation, largely due to lack of data, on the hydraulic properties of unsaturated organic soils in permafrost regions, and in particular, the relationship between hydraulic conductivity and pressure head. Additionally, there is uncertainty as to what fraction of the matrix and what pores conduct water at different pressure heads, as closed and dead-end pores are common features in organic soil. The objectives of this study were to determine the water-conducting porosity of organic soils for different pore radii ranges using the method proposed by Bodhinayake *et al.* (2004) [Soil Sci. Soc. Am. J. 68:760–769] and compare these values to active pore size distributions from resin-impregnated laboratory thin sections and pressure plate analysis. Field experiments and soil samples were completed in the Wolf Creek Research Basin, Yukon. Water infiltration rates were measured 16 times using a tension infiltrometer (TI) at 5 different pressure heads from -150 to 0 mm. This data was combined with Gardiner's (1958) exponential unsaturated hydraulic conductivity function to provide water-conducting porosity for different pore-size ranges. Total water-conducting porosity was $1 \cdot 1 \times 10^{-4}$, which accounted for only 0·01% of the total soil volume. Active pore areas obtained from 2-D image analysis ranged from 0·45 to 0·60, declining with depth. Macropores accounted for approximately 65% of the water flux at saturation, yet all methods suggest macropores account for only a small fraction of the total porosity. Results among the methods are highly equivocal, and more research is required to reconcile field and laboratory methods of pore and hydraulic characteristics. However, this information is of significant value as organic soils in permafrost regions are poorly characterized in the literature. Copyright © 2007 John Wiley & Sons, Ltd.

KEY WORDS   hydraulic conductivity; organic soils; tension infiltrometer; image analysis

Received 1 June 2006; Accepted 7 December 2006

INTRODUCTION

Organic soils dominate much of the subarctic and low-arctic regions, including tundra, taiga and wetlands (Soil Classification Working Group, 1998), and are composed of partially to well decomposed plant remains that have accumulated since the last glacial period. The saturated hydraulic properties of these soils have received particular attention in permafrost environments where organic soils are widespread due to low rates of decomposition and poor drainage of perennially frozen soils (Slaughter and Kane, 1979; Hinzman *et al.*, 1993; Quinton and Marsh, 1999; Carey and Woo, 2001). In these environments, saturated hydraulic conductivity and the mean hydraulic radii of the soil pores decline rapidly with depth within the organic layer, and hence the position of the water table largely governs the rate of subsurface water delivery from hillslopes to the stream (Quinton *et al.*, 2000; Carey and Woo, 2001). Models that relate the decline in pore hydraulic radii to hydraulic conductivity have been used to simulate runoff at the hillslope scale

in permafrost environments with some success (Quinton *et al.*, 2000; Quinton *et al.*, 2004).

Organic soils, like fractured geological media, have a dual porosity matrix (Loxham, 1980) consisting of active pores that conduct water through the soil matrix and inactive pores composed of closed and dead-end voids formed by the remains of plant cells (Hoag and Price, 1997). The total porosity, ϕ, of organic soils compared with mineral soils is typically quite large, reaching values up to 0·95 by volume, with much of the pore spaces classified as macropores ($>1 \times 10^{-3}$ m in diameter as defined by Luxmoore (1981)). The significance of larger macro and mesopores (defined as between 1×10^{-5} and 1×10^{-3} m in diameter by Luxmoore (1981)) is important in the rapid movement of water in and through organic soils. Only the continuous or interconnected pores contribute to the rapid flux of water observed in these soils. Hydraulic conductivity is governed by the diameter of the water-conducting pores, however, defining the diameter of an irregularly-shaped pore network common in organic soils is complex. The rate of flow through the pore is limited by the pore segments with the smallest diameter (i.e. bottlenecks) even though such bottlenecks may be only a small fraction of the total pore length (Dunn and

* Correspondence to: Sean K. Carey, Department of Geography and Environmental Studies, B349 Loeb Building, Carleton University, Ottawa, Ontario K1S 5A5, Canada. E-mail: sean_carey@carleton.ca

Phillips, 1991). Consequently, large pores do not necessarily imply higher hydraulic conductivity of bulk soil samples. More recently, the role of biogenic gas bubbles has been shown to have a large effect the saturated hydrologic conductivity of soils (Baird *et al.*, 2004), however, it is remains uncertain how this entrapped gas affects unsaturated hydraulic conductivity.

Traditionally, pore radii of the hydrologically active pores is determined via image analysis of thin sections (i.e. Boelter 1976; Hoag and Price, 1997; Quinton *et al.*, 2000; Fling and Flint, 2002). Active pores are classified as interconnected pores which can actively transmit water, as opposed to closed and dead-end pores formed by partially intact plant cell remains (Hayward and Clymo, 1982). Thin sections are prepared via acetone displacement and resin impregnation. Digital images are obtained directly from the impregnated soil blocks, or from thin sections, and imported into image analysis software as binary images. The active porosity, ϕ_a, is then computed as the inter-particle area expressed as a fraction of the total image area. Other methods such as computer assisted tomography scanning (Perret *et al.*, 2000) and gas diffusion (Bruckler *et al.*, 1989) exist but have not received widespread application. Static measurements of pore characteristics in the laboratory will not adequately describe the actual contributions to flow of water in soil (Messing and Jarvis, 1993). Consequently, *in situ* measurement of actual water-conducting porosity, ε, is essential in understanding the movement of water in the soil. Several techniques have been utilized to quantify the water-conducting porosity in field situations and of soil cores including: dye tracing (Bouma *et al.*, 1979; Weiler and Naef, 2003), tracers and breakthrough curves (Bouma and Wosten, 1979; Yeh *et al.*, 2000), and tension infiltrometer (TI) measurements at successive pressure heads (Watson and Luxmoore, 1986; Dunn and Phillips, 1991; Buttle and McDonald, 2000; Bodhinayake *et al.*, 2004).

Determination of active and water-conducting porosity and the associated pore diameter ranges, particularly for meso- and macropores, is important for characterizing both saturated and unsaturated hydraulic conductivity. However, the methods for determining active and water-conducting porosity and *in situ* hydraulic conductivity (both saturated and unsaturated) are not standard, and information on organic soils that have developed in cold regions is largely absent. Therefore, considering organic soils representative of permafrost regions, the objectives of this paper are to:

1. Determine the active porosity from laboratory thin sections and pressure plate analysis.
2. Quantify the water-conducting porosity using a TI at different pressure heads and determine the contributions of macropores to saturated flow.
3. Characterize pressure head—hydraulic conductivity relations *in situ* using a tension infiltrometer.

Results from this research will be useful in the formulation of algorithms predicting flow within organic soils and in improving overall hydraulic understanding of organic soils that form within cold regions.

STUDY SITE AND METHODS

Soil material and field experiments were conducted within Granger Basin (60° 32′ N, 135° 18′ W), a sub-catchment of the Wolf Creek Research Basin, Yukon Territory, Canada. Granger Basin is located approximately 15 km south of Whitehorse, Yukon Territory in the boreal Cordillera ecozone straddling the Southern Yukon Lakes and the Yukon-Stikine Highlands eco-regions (Pomeroy and Granger, 1999). Granger Basin elevation ranges from 1310 to 2250 m, is above treeline and Lewkowicz and Ednie (2004) approximate that 70% of the basin is underlain with permafrost. More detailed descriptions of Granger Basin and its hydrology can be found in Carey and Quinton (2004; 2005).

Field experiments were conducted on a north-facing slope with a continuous organic layer whose thickness decreases with distance upslope from ∼0·4 m in the valley bottom to ∼0·08 m near the crest (Quinton *et al.*, 2005). The upper ∼0·10 m, is composed of living *Sphagnum* vegetation and fibric peat. Below this, the peat is moderately to strongly decomposed. Three organic soil cores were extracted within a *ca.* 10 m² area near the middle of the slope, using 0·4 m lengths of clear PVC pipe (150 mm inner diameter) inserted in the ground vertically. The base of the tube was gently rotated into the ground, while a blade was used to cut downward into the peat around the outside of the tube. The procedure continued until the mineral substrate was reached. Before the core was removed from the ground, the compression factor was evaluated by measuring the difference in elevation of the top of the sample in the tube and the ground surface surrounding the outside of the core. In each case, the compression factor was found to be less than 10%. The soil from around the core was then excavated, the bottom of the core capped and the tube removed.

The three peat-filled tubes were returned to the laboratory where they were cut in half length-wise using a band saw. This procedure eliminated the need to remove the sediment from the tubes, and yielded a smooth face on both halves of each sample. On one half, three to five sub-samples were taken at evenly spaced intervals in order to measure the bulk density and total porosity. Total porosity, ϕ, was determined by the difference between saturated and dry soil weight of known volumes. The other half of each core was sent to the Department of Land Resource Science, University of Guelph, for acetone replacement and resin impregnation. Once the resin had hardened, sub-samples were removed and analysed for active porosity, ϕ_a, and mean pore diameters following the procedure described below. Water retention characteristic curves were obtained using data from standard pressure plate extractor tests performed at the Department of Geology and Geophysics, University of Calgary.

Samples were subject to eight levels of decreased matric potential (from 0·001 to 5 m) and at each moisture content were allowed to reach equilibrium and the sample was then weighed to determine volumetric soil moisture.

Two additional soil pits were excavated within the same *ca.* 10 m^2 area in order to obtain the soil moisture response to variations in soil tension using a pressure plate apparatus. In both pits, a 100 cm^3 sample was taken from the middle of the upper and lower layers for a total of 4 samples. Volumetric soil moisture was measured gravimetrically at nine increments of pressure head ranging between 0·001 (near saturation) to 5 m. Water retention characteristic curves were then fitted to the data using the approach of Van Genuchten (1980). Because of the irreversible changes to the soil structure during sample drying, the procedure was not repeated for the wetting phase.

Tension infiltrometer (TI) and water-conducting porosity

Infiltration measurements were performed between 15 and 23 August, 2005, using a TI (Soil Moisture Equipment Corp, Goleta, CA) with a 0·20-m diameter disk attached to the reservoir tower and tension control via a Marriott bubbler. Sixteen infiltration experiments were conducted within 10 m of the extracted soil samples on flat areas within the overall slope. At each location, shrub and herbaceous vegetation was cut back to the surface of the living organic layer and at eight locations; a fine layer of moist sand was applied beneath the porous disk. Contact material such as sand is recommended to smooth surface irregularities and improve contact between disk and the soil surface (Reynolds and Zebchuk, 1996). At eight alternate locations, the TI was placed directly on the prepared organic surface without a sand contact. Compression was minimized with a cradle device which dissipated the majority of the pressure away from the tension foot.

Infiltration measurements were performed with pressure heads of −150, −100−60, −30, and 0 mm from low to high pressure heads to reduce hysteresis where drainage occurs close to the disk while wetting continues near the wetting front (Reynolds and Elrick, 1991). The first pressure head was set to −150 mm and volume of water infiltrating the soil was measured by recording the water level drop in the graduated reservoir tower over time until stead-state infiltration was achieved, which occurred when the infiltration rate was unchanged over four measurement intervals (8 min). In general, steady state was achieved within 20−30 min. Following this, the pressure head was set at −100 mm and the above procedure completed for all the subsequent pressure heads. The reservoir was shielded from direct sunlight to prevent the formation of bubbles within the reservoir.

The steady-state infiltration rates obtained at different pressure heads were used to obtain field unsaturated hydraulic properties. For Gardner's (1958) exponential hydraulic conductivity function:

$$K(h) = K_{fs} \exp(\alpha_{GE}h) \qquad (1)$$

where $K(h)$ (LT^{-1}) is the unsaturated hydraulic conductivity for a given pressure head, h (L), K_{fs} is the field saturated hydraulic conductivity, and α_{GE} is the inverse macroscopic capillary length parameter (L^{-1}). Wooding (1968) derived an approximate solution for steady-state infiltration rate under a shallow disk

$$q_\infty(h) = \left(1 + \frac{4}{\alpha_{GE}\pi r_d}\right) K_{fs} \exp(\alpha_{GE}h) \qquad (2)$$

where q_∞ is the steady state infiltration rate (LT^{-1}) corresponding to the applied pressure head h, r_d is the radius of the tension disk (L). Equation (2) has two unknown parameters, K_{fs} and α_{GE}, that can be estimated through nonlinear regression of q_∞ as a function of h. Values for $K(h)$ are then estimated by substituting the resulting values into Equation (1). The equivalent radius $r(L)$ of the largest water-filled pore in the soil at a given pressure head h can be calculated from the capillary rise equation (Bear, 1972)

$$r = \frac{2\gamma \cos \beta}{\rho \, gh} \qquad (3)$$

Where γ is surface tension of water (MT^{-2}), β is the contact angle taken as 40° for moderately hydrophobic organic soils (Bachmann *et al.*, 2002; 2004), ρ is water density (ML^{-3}), g is gravity acceleration (LT^{-2}). In this study, it is assumed that the equivalent pores smaller than the r value estimated by Equation (3) are full of water and responsible for 100% of the water flux for a given pressure head. Furthermore, it is assumed that the equivalent pores larger than the value of r in Equation (3) are air-filled and do not contribute to any of the flux. According to Poiseuille's Law, the flow rate through a single vertical macropore due to gravity can be given as

$$Q(r) = \frac{\pi\rho \, g}{8\mu}r^4 \qquad (4)$$

where $Q(r)$ is the flow rate (L^3 T^{-1}) as a function of pore radius r and μ the dynamic viscosity of water (ML^{-1} T^{-1}).

Bodhinayake *et al.* (2004) derived in detail a new equation for determining water-conducting meso and macroporosity from TI measurements. This expands upon the previous methods of Watson and Luxmoore (1986) and Dunn and Phillips (1991) which assume a uniform pore-size distribution within the pressure head range, and linear dependence of hydraulic conductivity on pore radius. In brief, Bodhinayake *et al.* (2004) considered number of pores per unit area (L^2) as a function of pore radius r. The cumulative pore number distribution is given by

$$n(r) = \int_0^r P(r)dr \qquad (5)$$

where $n(r)$ is the total number of pores in a given pore size range and $P(r)$ is the number of pores per unit soil surface area per unit pore radius. The hydraulic

conductivity, $K(\text{L T}^{-1})$ at a given pore size r, $K(r)$ can be expressed as

$$K(r) = \int_0^r P(r)Q(r)dr \qquad (6)$$

where r is the upper limit of the integrals determining the pressure head. The water conducing porosity, ε, in a given range can be expressed as

$$\varepsilon(a, b) = \int_a^b \pi r^2 P(r)dr \qquad (7)$$

where a and b are pore radii (L). An expression for $P(r)$ is obtained by taking the derivatives of both sides of Equation (6). Substitution of $P(r)$ into Equation (7) yields

$$\varepsilon(a, b) = \int_a^b \frac{dK(r)}{dr} \frac{1}{Q(r)} \pi r^2 dr \qquad (8)$$

Typically, unsaturated hydraulic conductivity is expressed in relation to soil water content or pressure head. However, in Equation (8), the hydraulic conductivity is expressed as a function of pore radius. To express the hydraulic conductivity as a function of water pressure head, Equation (3) becomes

$$h(r) = \frac{2\gamma \cos \beta}{\rho \, gr} \qquad (9)$$

Where $h(r)$ is the water pressure head corresponding to radius r. Substitution of Equation (4) for $Q(r)$ and Equation (9) for r into Equation (8) provides

$$\varepsilon(a, b) = \frac{2\mu\rho \, g}{\gamma^2} \int_{h(a)}^{h(b)} \frac{dK(h)}{dh} h^2 dh \qquad (10)$$

and integration of Equation (10) by parts gives

$$\varepsilon(a, b) = \frac{2\mu\rho \, g}{\gamma^2} \left(h^2 K(h)\big|_{h(a)}^{h(b)} - 2\int_{h(a)}^{h(b)} K(h)h dh \right) \qquad (11)$$

Equation (11) is an exact equation for calculation of soil water-conducting porosity for a given range of pore radii or pressure heads. In this study, integration of Equation (11) was performed numerically by MathCad v. 13 (Math Soft, Cabridge, MA). Bodhinayake *et al.* (2004) present exact analytical solutions of Equation (11) for common hydraulic property functions like Gardner's exponential (1958) and rational (1965) functions, Brooks and Corey (1966) and Van Genuchten-Mualem (Van Genuchten, 1980). The total number of pores in a given pressure head, ΔN, assuming a constant r equal to the minimum pore radii can is taken as:

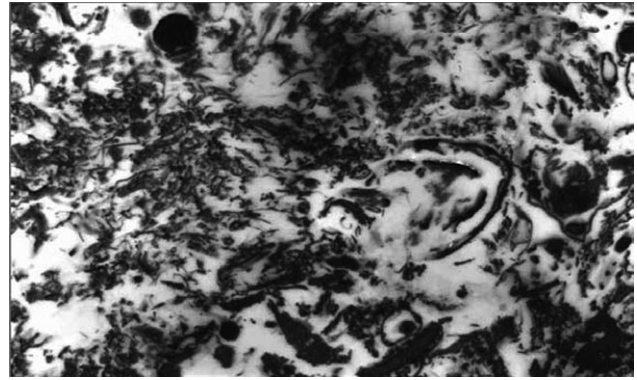$$\Delta N = \frac{\varepsilon(a, b)}{\pi a^2} \qquad (12)$$

Figure 1. Original digital black-and-white image of a soil thin section

Image analysis

Image analysis was completed on five sub-samples, two from each of the three resin impregnated cores using Sigma Scan pro 5 (SPSS Inc). Vertically oriented faces (side view of soil) with midpoints at 0·02, 0·035, 0·09, 0·10 and 0·15 m were polished and photographed using a high-resolution digital camera at the University of Guelph under ultra-violet light to provide enhanced contrast. The total area of the image ranged from 792 to 1363 mm^2. Digital images were converted to grey scale, with each pixel assigned a value between 0 (black) and 255 (white); where the lighter areas are pores and the darker areas soil (Figure 1). Following this, a threshold (also termed image segmentation) was assigned to pore and organic material areas (Thompson *et al.*, 1992). Unfortunately, due to the nature of organic material, a strong bi-modal distribution indicating pore and no-pore areas (i.e. Schaap and Lebron, 2001) was not obtained, and an alternate solution was required to assign a proper threshold. Compared to laboratory estimates of total porosity, visual inspection indicated that the binary overlay included non-pore areas. This problem occurred because the pores smaller than several pixels in size are either not resolved or are artefacts of the imaging process (Thompson *et al.*, 1992). The digital images have a resolution of 17 μm per pixel, and all features smaller than this cannot be resolved. To overcome this, an estimate of the porosity of the visible images was required. To this end, the water retention characteristic curve is required to estimate minimum pore radii. First, a smallest detectable pore size was established as an objected 2×2 pixels, with a corresponding diameter of about 34 μm and a hydraulic radius of 8·5 μm. Next, the water retention characteristic curves were used to determine the volume of pores smaller than the threshold size. The difference between this value and the saturated moisture content gives the approximate pore volume for the pressure-plate samples associated with the image analysis. The pore volume above the threshold size from the water characteristic curve was then used as the visible porosity for the image thresholding. Using Sigma Scan pro 5, a binary image was created by filling up the lighter (pore) areas to the visible porosity. The drawback of this method is the requirement that a threshold be obtained from the water

retention curve to define areas of the image that the program considers for measurement. Sigma Scan pro 5 measurement function was assigned to measure the area and perimeter of each pore. For each measurement, a hydraulic radius (r) was calculated using the capillary equation (Equation 3) and sorted in order of increasing radii. All pores smaller than the minimum hydraulic radii (8·5 μm) were removed from the data set.

RESULTS

Soil properties are summarized in Table I. The upper layer (0 to ~0·10 m) of organic soil consisted of living vegetation mixed with lightly decomposed peat and is classified as H2/H3 on the von Post scale (Soil Classification Working Group, 1998). Porosities were >90% by volume and bulk densities <100 kg m^{-3}. Below this, decomposition of the peat structure increased to H5/H6 on the von Post scale with some muddy residue within the matrix. Porosity declined with depth and bulk density increased as is typical in most organic soils (Chason and Siegel, 1986). The organic soil rests atop a mineral substrate consisting of a loamy-sand texture. Soil moisture for organic soil samples was plotted as a function of matric potential (data not shown) and a characteristic curve obtained utilizing the Van Genuchten equation (1980):

$$\theta(h) = \theta_r + \frac{(\theta_s - \theta_r)}{\left(1 + (\alpha_{vg}h)^n\right)^m} \tag{14}$$

where $\theta(h)$ is the volumetric moisture content at pressure h, θ_r is residual moisture content, θ_s is saturated moisture content and α_{vg}, m and n are fitting parameters where $m = 1-1/n$. θ_r and θ_s are obtained directly from the characteristic curve, whereas the other parameters are fitted by least squares error analysis. Parameter
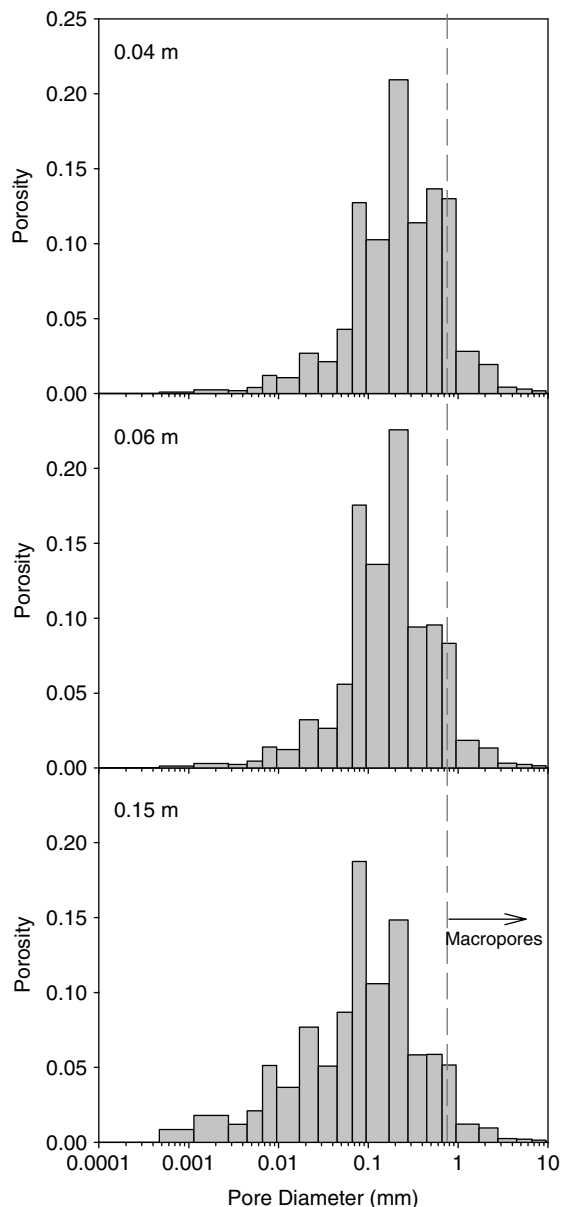

Figure 2. Frequencies of pore diameter distributions obtained from laboratory pressure plate analysis. The Van Genuchten (1980) unsaturated hydraulic conductivity function (Equation 13) was combined with Equation (3) to determine pore diameter, which were then grouped into ranges based on the image analysis thresholds. The vertical dashed line separates the macropores (right) from the mesopores (left)

values are reported in Table II and in all cases; curves fit the experimental data with an R^2 of 0·97 or better. On the basis of the pressure plate analysis, Equation (3) was then used to calculate pore size distributions (Figure 2).

Table I. Porosity and bulk density of organic soil for different depth. Values are mean and standard deviation

Depth (m)	Porosity (fraction)	Bulk density (kg m^{-3})
0·02	0·94 ± 0·03	40 ± 7
0·05	0·94 ± 0·04	68 ± 15
0·10	0·92 ± 0·06	81 ± 30
0·20	0·85 ± 0·07	141 ± 75
0·30	0·75 ± 0·11	290 ± 93

Table II. Curve-fitting parameters for Equation (13). θ_r is residual moisture content, θ_s is saturated moisture content and α_{vg}, m and n are fitting parameters where $m = 1-1/n$

Sample	1	2	3	4	5	6	7	8
Depth (m)	0·04	0·04	0·04	0·06	0·06	0·15	0·15	0·15
θ_r	0·14	0·14	0·16	0·19	0·17	0·22	0·18	0·25
θ_s	0·77	0·73	0·76	0·87	0·82	0·89	0·86	0·87
n	1·98	2·25	1·96	1·86	2·52	1·83	1·50	1·67
α_{vg}	38·56	31·57	37·22	37·98	18·28	18·36	25·09	18·82
m	0·50	0·56	0·49	0·46	0·60	0·45	0·34	0·40

There was a general trend towards reduced pore diameter and porosity with depth, and there are two dominant diameters (0·095 mm and 0·2767 mm) that are the most frequent pore size classes at all depths. Using the designation of Luxmoore (1981), macropores have a pressure range > -30 mm and mesopores -3000 to -30 mm. As $\beta = 0.4$ for organic soils in Equation (3), this provides an effective diameter range of 0·0076–0·76 mm for mesopores and >0.76 mm for macropores. Macroporosity was greatest at the 0·04 m accounting for 35% of the total soil porosity. This declines with depth, and at 0·15 m, macropores accounted for 16% of the soil volume.

Tension infiltrometer

Summary results for the 16 TI tests are presented in Table III and Figure 3. There was no spatial autocorrelation among the samples. As the sample sites were all nearby the sampling location for image analysis, catena related changes along the length of the entire slope were not evaluated. In most cases, the plots of the natural logarithm of steady state infiltration, $\ln Q_s$, against pressure head, h, were close to linear, allowing the application of Gardner's (1958) exponential function (Equation 1) to characterize unsaturated hydraulic conductivity. In just under half the cases, there was a break in slope between the -30 mm and 0 mm, indicating the dominance of macropores during saturated flow. This resulted in K_{fs} estimated via Equations (1) and (2) to be $5.49 \pm 2.67 \times 10^{-6}$ ms^{-1}, which is slightly less than the observed K_{fs} at $K(0$ mm) of $8.42 \pm 4.23 \times 10^{-6}$ ms^{-1}. The inverse capillary length parameter, α_{GE}, was 19 ± 0.06 m^{-1}, which compares well to those reported and cited for other soils (Reynolds et al., 2002), and a value of 27 m^{-1} calculated from Baird (1997, Table I) for peat soil. Values of $K(h)$ were very similar to organic soils reported by
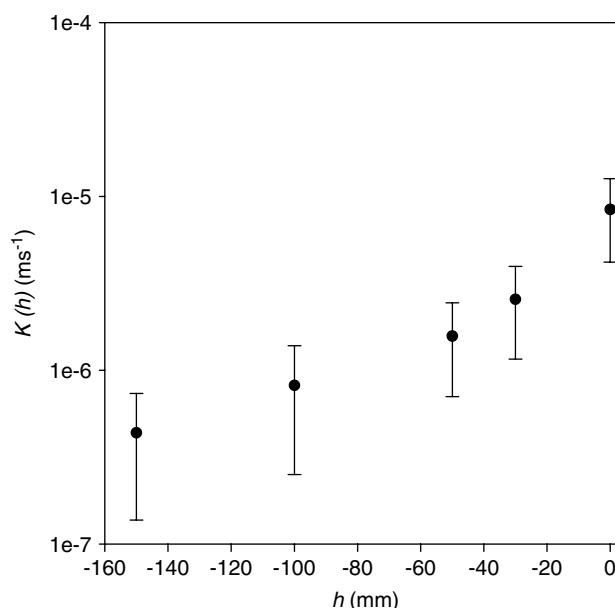

Figure 3. Plot of unsaturated hydraulic conductivity against pressure head determined from the tension infiltrometer. Dots are the man values and error bars represent ± 1 standard deviation

Baird (1997; Table I) and Holden et al. (2001; Figure 1). While definitions of macroporosity vary, a common characterization is pores >1 mm in diameter or -30 mm pressure head (Luxmoore, 1981) and the percentage of saturated flow due to macropore is often characterized as the difference between $K(0$ mm) and $K(-30$ mm) (Baird, 1997). Again, it is noted that a contact angle of $\beta = 0.4$ (Equation 3) is due to the hydrophobic nature of organic soil, which provides a slightly smaller pore diameter of 0·76 mm at -30 mm of pressure head versus a ~ 1 mm diameter when $\beta = 0$. As most previous studies for organic soils report the pressure head, this

Table III. Results of the TI tests. Samples 9 though 16 have a sand lens contact. SD is standard deviation and CV is the coefficient of variation

Sample	$K(-150$ mm$)$ ($\times 10^{-6}$ ms^{-1})	$K(-100$ mm$)$ ($\times 10^{-6}$ ms^{-1})	$K(-50$ mm$)$ ($\times 10^{-6}$ ms^{-1})	$K(-30$ mm$)$ ($\times 10^{-6}$ ms^{-1})	K_{fs} ($\times 10^{-6}$ ms^{-1})	Percent macropore
1	0·11	0·39	1·01	1·62	9·58	83·0%
2	0·41	0·32	0·85	1·61	2·93	45·1%
3	0·09	0·19	0·52	0·87	3·41	74·4%
4	1·14	1·63	2·58	2·84	9·75	70·8%
5	0·38	0·82	2·38	4·17	10·95	61·9%
6	0·05	0·41	0·72	0·85	2·73	68·8%
7	0·08	0·11	0·57	1·79	11·79	84·8%
8	0·69	2·19	3·67	6·50	14·60	55·5%
9	0·76	1·53	2·57	3·82	5·72	33·2%
10	0·39	0·57	1·62	2·89	10·88	73·4%
11	0·61	0·87	1·10	1·71	13·78	87·6%
12	0·29	0·50	1·14	2·13	5·61	61·9%
13	0·54	0·69	1·33	2·08	4·85	57·1%
14	0·53	0·86	1·84	2·93	3·62	19·0%
15	0·69	1·07	1·62	2·38	10·43	77·2%
16	0·23	0·93	1·64	2·74	14·12	80·6%
Mean	0·44	0·82	1·57	2·56	8·42	65%
SD	0·30	0·57	0·87	1·40	4·23	19%
CV	0·69	0·69	0·55	0·55	0·50	0·30

will be the basis of comparison. Macroporosity as determined from the TI was $65 \pm 19\%$ with values strongly skewed towards larger percentages. Seven of the tests had macropores accounting for over 80% of K_{fs}, whereas only two tests had values less than 50%. The largest macroporosity value was 88% and the smallest 19%. There was no significant difference between the samples with and without the sand contact lens ($p < 0.05$, Kolmogorov–Smirnov test), suggesting that a satisfactory contact can be obtained upon a carefully prepared organic surface. The variability in $K(h)$ as expressed by the coefficient of variation, CV, showed a general decline with decreased soil suction. CV declined from 69% at -150 mm to 55% at -30 mm, and the CV at K_{fs} is 50%. The range of variability was similar to that reported by other researchers on a variety of soil types. Watson and Luxmoore (1986) reported TI CV values of 95% for K_{fs}, and 72, 70 and 142% for pressure heads of -30, -60 and -150 mm respectively. Warrick and Nielsen (1980) suggested that CV for saturated mineral soils typically ranges between 100 and 200%, and is even greater for unsaturated soils. Reynolds *et al.* (2000) reported CVs using a TI that range from 60% to 164% for K_{fs}. In general, the CV was lower compared with mineral soil reported in the literature yet greater than those reported for organic soil by Baird (1997).

Water-conducting meso- and macroporosity given by Equation (11) for different pore diameter and pressure heads, along with the estimated number of pores from Equation (12), is presented in Table IV and Figure 4. The total water-conducting porosity, ε, for meso and macropores (pore diameter 0·0076 mm to 10 mm) is 0·011% of the total soil volume. On average, 65% of the total water flux occurs in pores larger than 0·76 mm (-30 mm pressure head), which accounted for only 1% (0·0001% of total soil volume) of the water-conducting porosity. Mesopores (pores 0·0076–0·76 mm) accounted for approximately 35% of the total water flux through 99% of the effective porosity (0·010% of soil volume). Although apparently quite small (see discussion), these values compare well with those reported by Dunn and Phillips (1991), Cameira *et al.* (2003) and Bodhinayake *et al.* (2004).

Image analysis

Active pore area fractions for the image threshold pore ranges indicated a general shift to smaller pore sizes with depth (Figure 5(a–f)). A notable exception was the 0·09 m image which had a high frequency of large pores, perhaps suggesting a low density zone below the surface that has been reported previously in some organic soils (Ingram, 1978; Hoag and Price, 1997). Deeper in the profile (5e, f), smaller pores dominated the effective pore area, confirming the long-standing observation of decreasing pore-radii with depth in soils. Macropores as a fraction of total effective pore area ranged from 2 to 59%. Note that the active pore area, ϕ_a, was approximately half that of the total porosity

Table IV. Estimated water-conducting porosity, fraction of total water-conducting porosity and number of pores in each pore diameter range

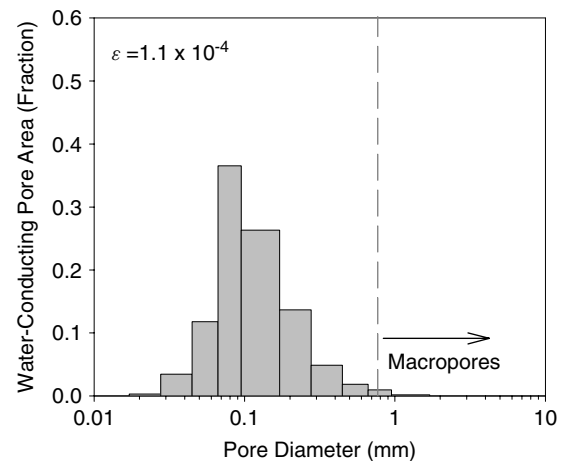| Pore diameter range (mm)	Water-conducting porosity ($\times 10^{-5}$)	Fraction of total water-conducting porosity	Number of pores (m^{-2})
0·0171–0·0277	0·00016	1.5×10^{-5}	27
0·0277–0·0448	0·0315	3.0×10^{-3}	1941
0·0448–0·0665	0·367	0·035	6772
0·0665–0·0949	1·25	0·118	9486
0·0949–0·171	3·89	0·365	18 260
0·171–0·277	2·80	0·264	3371
0·277–0·448	1·45	0·137	663
0·448–0·665	0·517	0·049	81
0·665–0·949	0·196	0·018	13
0·949–1·71	0·103	0·010	4
1·71–2·77	0·0192	1.8×10^{-3}	0·215
2·77–4·48	0·00492	4.6×10^{-4}	·021

Figure 4. Frequencies of total water-conducting porosity, ε, obtained from the tension infiltrometer for different pore diameter ranges. ε is the total water-conducting porosity. The vertical dashed line separates the macropores (right) from the mesopores (left)

determined from standard methods, and also decreased with depth as only pore spaces where resin is capable of impregnating is accounted for (Figure 5). The values of ϕ_a are approximately 20–25% less than estimated by Quinton *et al.* (2000) and are approximately twice that estimated by Hoag and Price (1997), although the method of determination is different in each case. A sharp transition occurred between near-surface blocks and those deeper within the profile, as the 0·1 m and 0·15 m (which are classified as lower samples) sample have only 2% of their total pore are consisting of voids within the macropore range. This contrasted samples closer to the surface which have macropores accounting for up to and exceeding one-half of the total pore diameters.

DISCUSSION

Organic soils have many distinct hydrological and hydraulic properties that present a challenge for hydro-
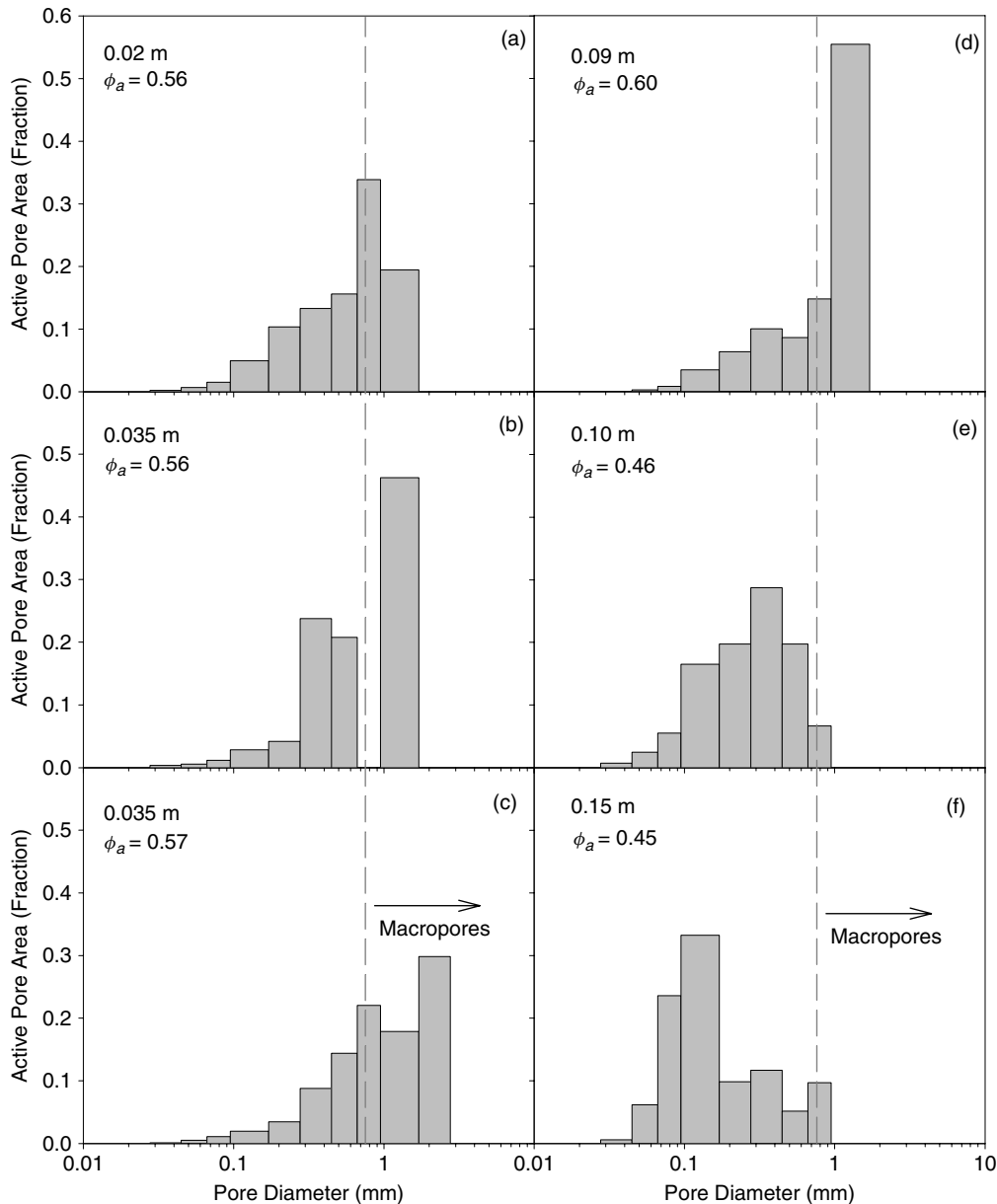
Figure 5. (a–f) Frequencies of the fractional active porosity, ϕ_a, obtained from the image analysis. ϕ_a is the total active porosity determined from the images. Panels a,b,c and d represent samples from the upper organic layer while e and f are from the lower layer. The vertical dashed line separates the macropores (right) from the mesopores (left)

logists. They are a compressible porous media whose properties such as porosity, specific retention and hydraulic conductivity change with wetness, depth and general state of decomposition, and entrapped gas content (i.e. Price and Schlotzhauer, 1999; Baird *et al.*, 2004; Kennedy and Price, 2005). Compared with mineral soils, and particularly agricultural soils, there has been less research on how these soils function, despite their widespread occurrence in arctic, subarctic and wetland environments. There has also been a shortage of standard analysis techniques such as water content versus matric suction data and the application of field-based instruments such as the Guelph permeameter (Hayashi and Quinton, 2004), TI (Baird, 1997; Holden *et al.*, 2001) and purpose-built infiltrometers (Bradley and Van Den Berg, 2005). In this study, three different techniques

were used to estimate hydraulic and pore characteristics for an organic soil overlying permafrost in subarctic Canada.

Field saturated and unsaturated hydraulic conductivity typically differ from lab estimates due to differences in sample size, flow geometry and various physical-hydrological characteristics (Bouma, 1982; Reynolds *et al.*, 2000). For the past 15 years, the TI has gained popularity for *in situ* measurement of near-saturated and saturated hydraulic properties because of its relative ease of use and that it causes little disturbance of the flow macrostructure, which controls near-saturated and saturated flow. However, to our knowledge only the study of Baird (1997) and Holden *et al.* (2001) have used the TI on organic soils in a field setting. Results from this experiment provide K_{fs} values that are approximately

one order of magnitude lower than most reported for similar permafrost-underlain organic soils, yet are similar to those of Baird (1997) and Holden *et al.* (2001). Quinton *et al.* (2000) reported values of K_{fs} from a constant head permeameter of 5×10^{-4} ms^{-1} and values from lateral breakthrough of tracers ranging from 10^{-2} to 10^{-4} ms^{-1} depending upon depth. Carey and Woo (2001) using slug and bail tests reported a K_{fs} from 10^{-3} to 10^{-4} m s^{-1} depending upon depth for similar organic soil profiles within the Wolf Creek Research Basin. Carey and Quinton (2005) provide tracer breakthrough results of K_{fs} for a plot immediately adjacent to the TI tests in this site, with values declining from 10^{-3} ms^{-1} at 10 cm to 10^{-5} ms^{-1} at 0·3 m. Considering that the TI rests atop the surface, it is surprising the low values of K_{fs} compared with most previous methods. However, organic soils are highly anisoptropic, having saturated hydraulic conductivity values greater in the horizontal than vertical direction (Chason and Siegel, 1986). The majority of previous field experiments have reported horizontal K_{fs}, and Beckwith *et al.* (2003) reports anisotropy in peat soils and its variability with depth, and points out that vertical K_{fs} is less than horizontal in most cases, and that it exhibits much less variability with depth. These results may in part explain the lower values of K_{fs} observed from the TI. Furthermore, two additional possibilities aside from measurement error (discussed below) exist: 1) gas entrapped in the peat matrix may inhibit the vertical movement of water (Reynolds *et al.*, 1992), and 2) infiltration is limited by the smaller pore radii at depth, restricting rapid water movement and enhancing the production of percolation-restricted lateral runoff widely cited as a rapid runoff response mechanisms in cold regions dominated by organic soils (i.e. McNamara *et al.*, 1998; Quinton and Marsh, 1999; Carey and Woo, 2001).

The use of a contact material has been highlighted as necessary to maintain a good and consistent hydraulic contact between the infiltrometer membrane and the soil (Reynolds and Zebchuk, 1996). However, in the two previously reported application of the TI on organic soils, Holden *et al.* (2001) used contact sand, whereas Baird (1997) did not. Despite this, their results are quite similar and the eight replicates for sand and no-sand contact in this study showed no significant difference for the grouped $K(h)$ data. It is likely that due to the spongy nature of the peat surface, a good contact can be obtained on a carefully prepared surfaces the pressure of the TI slightly depresses the surface and the organic material closely moulds to the porous disk. The use of contact material is a critical and perhaps limiting issue in organic soils as $K(h)$ of the contact material should be less than the test material (Reynolds and Elrick, 1991); a guideline that is difficult to satisfy for highly porous organic material.

When considering macropores, the total fraction of their soil occupied by them (macroporosity) and the amount of water they conduct is important. The percentage of macropore flow contribution to K_{fs} as determined from the TI ranged from 19 to 86%, and was approximately 10–15% higher than those observed to *Sphagnum* peat soils in the United Kingdom, despite differences in organic thickness and degree of humification (Baird, 1997; Holden *et al.*, 2001). In this study, organic soils were thinner and less humified than those reported in the United Kingdom, possibly explaining the greater fraction of macropore contribution. Holden *et al.* (2001) reported macroporosity for different peat vegetation types and a different depth, noting that *Sphagnum* had the highest macroporosity (*ca.* 50%) that showed little variability with depth. Despite the large water flux attributed to macropores at saturation, it is unclear as to what volume of the soil contributes to this flux. From Poisuelle's Law (Equation 4), a macropore of 1 mm equivalent diameter can transmit as much flow as 16 macropores with a 0·5 mm diameter and 10 000 macropores with a diameter of 0·1 mm. Total water-conducting porosities are summarized in Table III for the pore diameter ranges in which the image analyses thresholds were performed. Application of Equation (12) between pore diameters of 0·76 mm and 10 mm provides 30 pores and a water-conducting porosity of only 0·00023% of the total soil volume. Calculating water-conducting porosity using the methods of Watson and Luxmoore (1986) and Dunn and Phillips (1991) (equations not presented) provide estimates of ε up to one order of magnitude greater (0·0013% and 0·00076% respectively), yet the theoretical underpinning of these models is less robust as that presented by Bodhinayake *et al.* (2004). The total water-conducting porosity accounts for only 0·01% of the total soil volume, or approximately 0·02% of the active porosity determined from image analysis. While it appears that the water-conducting porosity is very low, Bouma *et al.* (1979) reports that water-conducting macropores often occupy <1% of the total soil volume.

The volume of pore areas (active and water conducting) differs among the methods, which is unsurprising considering the mixing of two and three dimensional estimates of pore characteristics. Regardless, it is instructive to compare the cumulative ratio of the total active and water-conducting porosity with pore diameter (Figure 6). The method of application has a large influence upon the characterization of porosity and the extent to which macropores are present and functioning within the matrix. Grouping the upper and lower image samples for clarity with the pressure plate and TI data, there is a wide range in predicted cumulative pore fractional areas. While the absolute water-conducting pore area is several orders of magnitude smaller than the active pore area, the cumulative fractional ε does not follow the same distribution as ϕ_a. Figure 6 implies that smaller pores between 0·05 and 0·1 mm are the most available in transmitting water (although they transmit small volumes of water), despite image and pressure plate analysis suggesting that below 0·1 mm, there is only a small fraction of
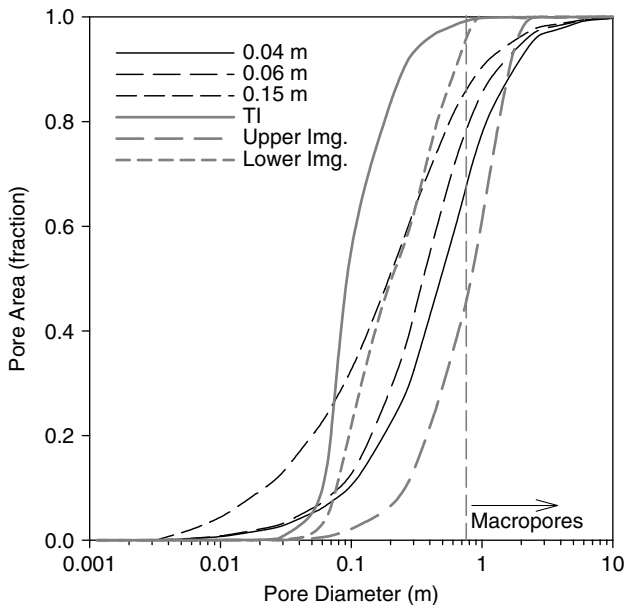
Figure 6. Cumulative fractional pore areas (ϕ_a and ε) as determined from pressure plate analysis, image analysis and tension infiltrometer (TI). Upper Img. refers to the grouped 0·02–0·09 m samples and Lower Img. the grouped 0·10 and 0·15 m image. The vertical dashed line separates the macropores (right) from the mesopores (left)

active pores (<10% of ϕ_a) near the surface. Thus, even near saturation when large pores begin to fill, the vast majority of these pores do not conduct water. A potential explanation is that smaller pores exhibit a greater degree of interconnectivity than larger pores. At depth, this active pore area fraction increases to approximately 40%. Intriguingly, there is a closer correspondence in parameter distributions between the TI and image/tension samples at depth despite the TI being placed on the surface. The pressure plate analysis is able to resolve a greater range of pore diameters than the image analysis which is restricted to a minimum pore diameter of 34 μm

Experimental limitations

There are several important issues associated with the data collection. With regards to the TI data and analysis: (i) it is assumed that the $K(h)$ prior to the experiment is much less than the hydraulic conductivity imposed under the initial tension $K(-150 \text{ mm})$, although this theoretical limitation may produce only minor errors (Reynolds and Elrick, 1991). (ii) Wooding's (1968) solution for infiltration from a shallow pond assumes the soil beneath the tension disc is homogeneous, isotropic and uniformly unsaturated. For the vast majority of TI measurements reported in the literature, these assumptions are rarely met. While soil properties do change with depth, the critical point is whether the peat properties change significantly within the zone of influence of the tension disk. The greatest flux of water entering the soil was during any experiment was 1·48 L, which results in a uniform infiltration depth of 46 mm under the disk. However, this water depth does not indicate how deep the wetting front bulb had penetrated and with the reduced active and

water-conducting porosity, water would have infiltrated to greater depth. (iii) It is unclear as to what role the hydrophobicity of organic soil plays on TI measurements. (iv) The method of Bodhinayake *et al.* (2004) assumes pores are smooth cylindrical capillary tubes and laminar water flow in large macropores. In reality, pores have irregular shapes and water flow in some large macropores may be turbulent. (v) A parametric model of $K(h)$ is required. In this case, Gardner's (1958) model was chosen due to its widespread application and appropriate fit to the field data, although other $K(h)$ functions can be use where appropriate (i.e. Brooks and Corey, 1966; Gardner 1965; Van Genuchten, 1980). (vi) Cryoturbation affects the properties of the soils through time, although it is difficult to assess from this study what the implications are on $K(h)$. With regards to the image analysis: (i) the lower resolution of pores was a diameter of 34 um; any pore below that was irresolvable. (ii) Owing to the optical properties of organic material and the resin, a strong bi-modal optical distribution in the image analysis was not obtained. To overcome this, water retention characteristic curves were used to bound the volume of active pores for different diameter thresholds. It would be beneficial to overcome this dependency by using a resin that is readily distinguished from the organic soil matrix.

CONCLUSION

In this study, three different techniques were used to estimate hydraulic and pore characteristics of organic soils typical to permafrost regions of northern Canada. Field-based measurements using a TI of unsaturated and saturated hydraulic conductivity were similar to *Sphagnum* soils in the United Kingdom, although K_{fs} was up to several orders of magnitude lower than horizontal K_{fs} estimated from tracer breakthrough and pump/bail tests previously reported for these soils (Carey and Woo, 2001; Carey and Quinton, 2005). Gardner's (1958) exponential unsaturated hydraulic conductivity function was an appropriate model for K versus h relations and macropores (pores ranging from 0·76 mm to 100 mm in diameter) are considered responsible for approximately 64% of the total water flux at saturation. With regards to pore and flow characteristics, results were highly equivocal as methods do not directly compare in both the pores property being measured and in their dimension of measurement (2-D vs. 3-D). Water-conducting porosity as determined by the TI was only 0·01% of the total soil volume; several orders of magnitude less than the active and total porosity determined from image and laboratory analysis. This implies that only a very small fraction of the total pores are responsible for the flux of water. This study provides extremely useful base-line data on pore and hydraulic properties of permafrost-underlain organic soils, yet continued laboratory and field experiments are required before their hydrological characteristics are fully resolved.

REFERENCES

Bachmann J, Horton R, Grant SA, Van der Ploeg RR. 2002. Temperature dependence of water retention curves for wettable and water-repellent soils. *Soil Science Society of America Journal* **66**: 44–52.

Bachmann J, Woche SK, Goebel MO, Kirkham MB, Horton R. 2004. Extended methodology for determining wetting properties of porous media. *Water Resources Research* **39**. DOI: 10.1029/2003WR002143.

Baird AJ. 1997. Field estimation of macropore functioning and surface hydraulic conductivity in a fen peat. *Hydrological Processes* **11**: 287–295.

Baird AJ, Beckwith CW, Waldron S, Waddington JM. 2004. Ebullition of methane-containing gas bubbles from near-surface *Sphagnum* peat. *Geophysical Research Letters* **31**. DOI: 10.1029/2004GL021157.

Bear J. 1972. *Dynamics of Fluids in Porous Media*. Elsevier: New York.

Beckwith CW, Baird AJ, Heathwaite AL. 2003. Anisotropy and depth-related heterogeneity of hydraulic conductivity in a bog peat. I: laboratory measurements. *Hydrological Processes* **17**: 89–101.

Bodhinayake WL, Si BC, Xiao C. 2004. New method for determining water-conducting macro- and mesoporosity from tension infiltrometer. *Soil Science Society of America Journal* **68**: 760–769.

Boelter DH. 1976. Methods for analyzing the hydrological characteristics of organic soils in marsh-ridden areas. *Hydrology of Marsh-Ridden Areas. Proceedings IASH Symposium. Minsk, 1972*, IASH, UNESCO: Paris, 161–169.

Bradley C, Van Den Berg JA. 2005. Infiltration mechanisms in a herbaceous peat: results of a controlled infiltration experiment. *Hydrological Sciences Journal* **50**: 713–725. doi: 10.1623/hysj.2005.50.4.713.

Brooks RH, Corey AT. 1966. Properties of porous media affecting fluid flow. *Journal of Irrigation and Drainage Division, American Society of Civil Engineers* **92**(IR2): 71–88.

Bruckler B, Ball C, Renault P. 1989. Laboratory estimation of gas diffusion coefficient and effective porosity in soils. *Soil Science* **147**: 1–10.

Bouma J. 1982. Measuring the hydraulic conductivity of soil horizons with continuous macropores. *Soil Science Society of America Journal* **46**: 438–441.

Bouma J, Wosten JHM. 1979. Flow patterns during extended saturated flow in two undisturbed swelling clay soils with different macrostructures. *Soil Science Society of America Journal* **43**: 16–22.

Buttle JM, McDonald DJ. 2000. Soil macroporosity and infiltration characteristics of a forest podzol. *Hydrological Processes* **14**: 831–848.

Cameira MR, Fernando RM, Periera LS. 2003. Soil macropore dynamics affected by tillage and irrigation for silty loam alluvial soil in southern Portugal. *Soil and Tillage Research* **70**: 131–140.

Carey SK, Woo M-K. 2001. Slope runoff processes and flow generation in a subarctic, subalpine environment. *Journal of Hydrology* **253**: 110–129.

Carey SK, Quinton WL. 2004. Evaluating snowmelt runoff generation in a discontinuous permafrost catchment using stable isotope, hydrochemical and hydrometric data. *Nordic Hydrology* **35**: 309–324.

Carey SK, Quinton WL. 2005. Evaluation of runoff generation during summer using hydrometric, stable isotope and hydrochemical methods in a discontinuous permafrost environment. *Hydrological Processes* **19**: 95–114.

Chason DB, Siegel DI. 1986. Hydraulic conductivity and related properties of peat, lost river peatland, Northern Minnesota. *Soil Science* **142**: 92–99.

Soil Classification Working Group. 1998. *The Canadian System of Soil Classification*. Agriculture and Agri-Food Can. Publ. 1646 (Revised), NRC Research Press: Ottawa, 187.

Dunn GH, Phillips RE. 1991. Macroporosity of a well-drained soil under no-till and conventional tillage. *Soil Science Society of America Journal* **55**: 817–823.

Fling LE, Flint AL. 2002. The soil solution phase. Porosity. In *Methods of Soil Analysis. Part 4.*, Dane JH, Topp GC (eds). Soil Science Society of America: Madison, Wisconsin, 241–245.

Gardner WR. 1958. Some steady-state solutions of unsaturated moisture flow equations with application to evaporation from a water table. *Soil Science* **85**: 228–232.

Gardner WR. 1965. Dynamics of soil-water availability to plants. *Annual Review of Plant Physiology* **16**: 323–342.

Hayashi M, Quinton WL. 2004. A constant-head well permeameter method for measuring field-saturated hydraulic conductivity above an impermeable layer. *Canadian Journal of Soil Science* **84**: 255–264.

Hayward PM, Clymo RS. 1982. Profiles of water content and pore size in sphagnum and peat, and their relation to bog ecology. *Proceedings of the Royal Society of London Series B* **215**: 299–325.

Hinzman LD, Kane DL, Everett KR. 1993. Hillslope hydrology in an arctic setting. *Proceedings, Sixth International Conference on Permafrost*, South China Press: Beijing, 257–271.

Hoag RS, Price JS. 1997. The effects of matrix diffusion on solute transport and retardation in undisturbed peat in laboratory columns. *Journal of Contaminant Hydrology* **28**: 193–205.

Holden J, Burt TP, Cox NJ. 2001. Macroporosity and infiltration in blanket peat: the implications of tension disk infiltrometer measurements. *Hydrological Processes* **15**: 289–303.

Ingram HAP. 1978. Soil layers in mires: function and terminology. *Journal of Soil Science* **29**: 213–218.

Kennedy GW, Price JS. 2005. A conceptual model of volume-change controls on the hydrology of cutover peats. *Journal of Hydrology* **302**: 13–27.

Lewkowicz AG, Ednie M. 2004. Probability mapping of mountain permafrost using the BTS method, Wolf Creek, Yukon Territory, Canada. *Permafrost and Periglacial Processes* **15**: 67–80.

Loxham M. 1980. Theoretical considerations of tansport of pollutants in peat. In *Proceedings, 6th International Peat Congress*, Duluth MN, 600–606.

Luxmoore RJ. 1981. Micro-, meso-andmacroporosity of soil. *Soil Science Society of America Journal* **45**: 671–672.

McNamara JP, Kane DL, Hinzman LD. 1998. An analysis of streamflow hydrology in the Kuparuk River Basin, Arctic Alaska: a nested watershed approach. *Journal of Hydrology* **206**: 39–57.

Messing I, Jarvis NJ. 1993. Temporal variation in the hydraulic conductivity of a tilled clay soil as measured by tension infiltrometers. *Journal of Soil Science* **44**: 11–24.

Perret J, Prasher SO, Kantzas A, Langford C. 2000. A two-domain approach using CAT scanning to model solute transport in soil. *Journal of Environmental Quality* **29**: 995–1010.

Pomeroy JW, Granger RJ. 1999. *Wolf Creek Research Basin: Hydrology, Ecology, Environment*. Environment Canada: Saskatoon, 160.

Price JS, Schlotzhauer SM. 1999. Importance of shrinkage and compression in determining water storage changes in peat: the case of a mined peatland. *Hydrological Processes* **13**: 2591–2601.

Quinton WL, Marsh P. 1999. A conceptual framework for runoff generation in a permafrost environment. *Hydrological Processes* **13**: 2563–2581.

Quinton WL, Gray DM, Marsh P. 2000. Subsurface drainage from hummock-covered hillslopes in the Arctic tundra. *Journal of Hydrology* **237**: 113–125.

Quinton WL, Carey SK, Goeller NT. 2004. Snowmelt runoff from northern alpine tundra hillslopes: major processes and methods of simulation. *Hydrology and Earth System Sciences* **8**: 877–890.

Quinton WL, Sharizi T, Carey SK, Pomeroy JW. 2005. Soil Water Storage and active layer development in a sub alpine tundra hillslope, southern Yukon Territory, Canada. *Permafrost and Periglacial Processes* **16**: 369–382.

Reynolds WD, Elrick DE. 1991. Determination f hydraulic conductivity using a tension infiltrometer. *Soil Science Society of America Journal* **55**: 633–639.

Reynolds WD, Zebchuk WD. 1996. Use of contact material in tension infiltrometer measurements. *Soil Technology* **9**: 141–159.

Reynolds WD. Elrick DE, Youngs EG. 2002. The soil solution phase. Single-ring and double- or concentric-ring infiltrometers. In *Methods*

of soil analysis. Part 4., Dane JH, Topp GC (eds). Soil Science Society of America: Madison, Wisconsin, 821–826.

Reynolds WD, Brown DA, Mathur SP, Overend RP. 1992. Effect of *in situ* gas accumulation on the hydraulic conductivity of peat. *Soil Science* **153**: 397–408.

Reynolds WD, Bowman BT, Brunke RR, Drury CF, Tan CS. 2000. Comparison of tension infiltrometer, pressure infiltrometer, and soil core estimates of saturated hydraulic conductivity. *Soil Science Society of America Journal* **64**: 478–484.

Schaap MG, Lebron I. 2001. Using microscope observations of thing sections to estimate permeability with the kozeny-carman equation. *Journal of Hydrology* **251**: 186–201.

Slaughter CW, Kane DL. 1979. Hydrologic role of shallow organic soils in cold climates. *Proceedings, Canadian Hydrology Symposium 79—Cold Climate Hydrology*, National Research Council of Canada: Ottawa, 380–389.

Thompson ML, Singh P, Corak S, Straszheim WE. 1992. Cautionary notes for the automated analysis of soil pore-space images. *Geoderma* **53**: 399–415.

Van Genuchten MT. 1980. A closed form equation for predicting the hydraulic conductivity of unsaturated soils. *Soil Science Society of America Journal* **44**: 892–898.

Watson KW, Luxmoore RJ. 1986. Estimating macroporosity in a forest watershed by use of a tension infiltrometer. *Soil Science Society of America Journal* **50**: 578–582.

Warrick AW, Nielsen DR. 1980. Spatial variability of soil physical properties in the field. In *Applications of Soil Physics*, Hillel D (ed). Academic Press: New York.

Weiler M, Naef F. 2003. An experimental tracer study of the role of macropores in infiltration in grassland soils. *Hydrological Processes* **14**: 477–493.

Wooding RA. 1968. Steady infiltration from a shallow circular pond. *Water Resources Research* **4**: 1259–1273.

Yeh YJ, Lee CH, Chen ST. 2000. A tracer method to determine hydraulic conductivity and effective porosity of saturated clays under low gradients. *Ground Water* **38**: 522–529.